

Robust passive range estimation using the waveguide invariant

Kevin L. Cockrell^{a)} and Henrik Schmidt

Department of Mechanical Engineering, Massachusetts Institute of Technology, 77 Massachusetts Avenue, Cambridge, Massachusetts 02139

(Received 30 September 2009; revised 26 January 2010; accepted 3 February 2010)

The waveguide invariant principle is used to estimate the range to a broadband acoustic source in a shallow-water waveguide using a single acoustic receiver towed along a path directly toward the acoustic source. A relationship between the signal processing parameters and the ocean-acoustic environmental parameters is used to increase the effective signal-to-noise ratio without requiring detailed knowledge of the environment. Heuristics are developed to estimate the minimum source bandwidth and minimum horizontal aperture required for range estimation. A range estimation algorithm is tested on experimental and simulated data for source ranges of 500–2200 m and frequencies from 350 to 700 Hz. The algorithm is accurate to within approximately 25% for the cases tested and requires only a minimal amount of *a priori* environmental knowledge.

© 2010 Acoustical Society of America. [DOI: 10.1121/1.3337223]

PACS number(s): 43.30.Wi, 43.60.Gk, 43.60.Jn, 43.30.Bp [AIT]

Pages: 2780–2789

I. INTRODUCTION

Most research on acoustic source localization in the ocean has focused on using coherent signal processing techniques such as matched field processing¹ (MFP). While MFP works well in theory and in numerical simulation, it is not always applicable to real-world situations because it requires very accurate knowledge of the environment (e.g., sound speed profile and acoustic properties of the sea floor) in order to correctly localize the source.

Other source localization methods have been developed that require much less *a priori* knowledge about the environment by using the concept of the waveguide invariant. The waveguide invariant has been applied to estimating the range to acoustic sources in various circumstances using a variety of signal processing schemes such as the following:

- Estimating the range to a fixed acoustic source from measurements taken by a vertical hydrophone array by analyzing the MFP sidelobe behavior,² and
- estimating the closest point of approach of a moving source to a single fixed hydrophone using a Hough transform-like technique.³

In the present work, a technique is developed to estimate the range to a fixed acoustic source from the acoustic intensity as measured over a window of ranges and frequencies, $I(r, f)$. The technique is tested on experimental data that was obtained from an acoustic receiver towed by an autonomous underwater vehicle heading directly toward the acoustic source. Previous research papers have used the two-dimensional discrete Fourier transform (2D-DFT) of $I(r, f)$ to estimate the value of the waveguide invariant when the source range was known.^{4,5} This paper extends that research

to using the 2D-DFT of $I(r, f)$ to perform range estimation and develops guidelines for choosing the signal processing parameters' values.

The objective of the present work is to investigate the issues related to the signal processing that is required for range estimation using the 2D-DFT of $I(r, f)$ in the context of performing the estimation autonomously (i.e., without requiring human interpretation of any images) and to perform the range estimation on simulated and experimental data. The main results are the following.

- The minimum bandwidth of the acoustic source and minimum range window of acoustic intensity measurements required for accurate range estimation can be determined from a modest knowledge of the acoustic waveguide parameters before any acoustic measurements are made.
- A relationship between the signal processing parameters and the ocean-acoustic waveguide parameters can be used to reject much of the noise present in experimental data.
- Range estimation can be performed robustly, requiring very little *a priori* environmental knowledge (at least, for the data sets analyzed this paper).
- A range estimate accuracy of approximately 25% is achieved with the experimental data set used in the present analysis.

Section II discusses the waveguide invariant concept. In Sec. III, the range estimation algorithm based on a 2D-DFT is discussed. Section IV applies the algorithm to simulated and experimental data. And finally, Sec. V gives a summary and conclusion.

II. THE WAVEGUIDE INVARIANT

A plot of acoustic intensity versus range and frequency, $I(r, f)$, due to a broadband source in a waveguide exhibits striations. The striations are due to the functional dependence of the intermodal interference length on frequency and are characterized by the value of the waveguide invariant.⁶ Sev-

^{a)}Author to whom correspondence should be addressed. Electronic mail: cockrell@mit.edu

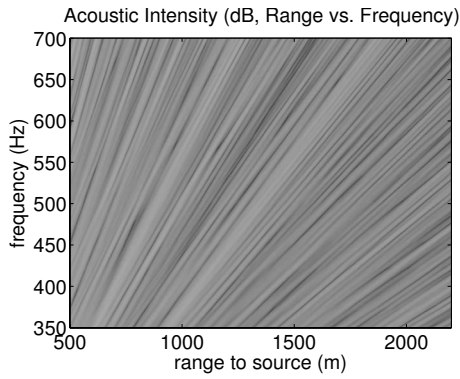


FIG. 1. Acoustic intensity (dB, arbitrary reference) in a Pekeris waveguide plotted versus range and frequency, $I(r, f)$, for a receiver depth of 20 m and a source depth of 40 m.

eral references derive the waveguide invariant.^{2,5,7} This paper skips the derivation of the waveguide invariant and focuses on the interpretation of it. The waveguide invariant's striations can be seen in Fig. 1, which is a plot of the simulated acoustic intensity in a 100 m deep Pekeris waveguide with a water sound speed of 1500 m/s and a bottom sound speed and density of 1700 m/s and 1750 kg/m³, respectively.

Using normal modes to describe the acoustic field in a waveguide, the acoustic intensity can be approximated as⁷

$$I(r, f) \propto \sum_{n=1}^{n=M} \sum_{m=1}^{m=M} B_m B_n \cos(\Delta \xi_{mn}(f)r), \quad (1)$$

where M is the number of propagating modes, B_m and B_n are the modal amplitudes, and $\Delta \xi_{mn}(f)$ is the difference in the acoustic horizontal wavenumbers between mode m and mode n , which is a function of frequency. Note that this approximation does not include the $1/r$ spreading.

Each cosine term of the summation in Eq. (1) is a result of two modes interfering and causes striations in $I(r, f)$. The slopes of the striations depend on the range r , the frequency f , and how the difference between the two modes' horizontal wavenumbers depends on frequency (which is characterized by the waveguide invariant β). Specifically, the slope of any given striation in $I(r, f)$ approximately obeys the relation⁷

$$\frac{\delta f}{\delta r} = \beta \frac{f}{r}, \quad (2)$$

where $\delta f / \delta r$ is the slope and β is the waveguide invariant.

The value of β is unique for each mode pair because each mode pair's horizontal wavenumber difference can have a different dependence on frequency, but the reason β is said to be invariant is because the value of β is approximately the same most mode pairs, under certain circumstances.

It can be shown analytically that $\beta \approx 1$ in an ideal waveguide for mode pairs where both modes are far from cutoff.⁷ $\beta \approx 1$ for most Pekeris waveguides as well because the modes far from cutoff in a Pekeris waveguide behave similarly to the modes far from cutoff in an ideal waveguide. It is instructional to look at Fig. 1 and verify that Eq. (2) is (approximately) true using $\beta = 1$. That relationship between the slopes of the striations and the range to the source will be used to estimate the range to the acoustic source.

The value of β that will be observed in a striation pattern depends on the sound speed profile, the seafloor properties, and the source and receiver locations. Authors in Refs. 2, 4, 8, and 9 discuss this in more detail, but empirical evidence and numerical models suggest that for mode pairs where both modes interact with the top and the bottom of the waveguide, $\beta \approx 1$. So if the acoustic intensity is dominated by modes that interact with the top and bottom of the waveguide, the β observed in the striation pattern will likely be close to 1. Throughout this paper, for both the simulated and experimental data, we assume $\beta = 1$. The consequences of this assumption being incorrect are discussed shortly.

To use Eq. (2) for range estimation, it is rewritten as

$$r = \beta \cdot f \cdot \frac{\delta r}{\delta f}, \quad (3)$$

which allows for one to estimate the range of the acoustic source if one measures the slopes of the striations and assumes a value of β . The effect of assuming an incorrect value of β can be seen in Eq. (3). If the true value of β is β_{true} and the assumed value is β_{assumed} , then the range estimates will be incorrect by a factor of $\beta_{\text{assumed}} / \beta_{\text{true}}$.

In order to estimate the range to the source, one begins by calculating $I(r, f)$ for some range of values of r and f . In a simulation one can calculate $I(r, f)$ in the frequency domain using acoustic simulation software. In an experiment, one must estimate the power spectrum of a hydrophone's time series at several ranges. In practice, $I(r, f)$ will likely be the spectrogram of a time series of acoustic pressure obtained by moving an acoustic receiver radially toward or away from the acoustic source, as is done in Sec. IV B.

To estimate the source's location, one then must determine the slopes of the striations (or curved paths of the striations, if $\beta \neq 1$) in $I(r, f)$. Because of the visually striking relationship between the striation slope and the source's location, a person looking at $I(r, f)$ can estimate the source's location rather easily. However, the present work focuses on techniques that perform the range estimation autonomously (i.e., without the benefit of having a person to visually interpret $I(r, f)$ or its 2D-DFT).

III. USING THE TWO-DIMENSIONAL DISCRETE FOURIER TRANSFORM FOR RANGE ESTIMATION

A. Outline

The slope of the striation, $\delta f / \delta r$, at a particular range-frequency combination (r, f) can be inserted into Eq. (3) to estimate the range to the source. The technique described in this section to determine the slope of a striation in $I(r, f)$ looks at a small local region (a "window") of $I(r, f)$ and assumes that all of the striations within that window have the same slope. This is similar to what is done Refs. 4, 5, and 10 but in those papers the ranges were much larger than the ranges used in the present analysis, so the slopes of the striations did not change quickly with range. Consequently, those papers did not focus much attention on how to choose the size of the window. Because of the short ranges used in the present analysis, the slopes change quickly with range and so much care must be given in choosing the window size in

order to ensure that the slopes do not change too much inside of the window. This issue is discussed in Sec. III B 4.

In addition to the striations from the source, $I(r, f)$ will also contain noise which can be partially eliminated by filtering. The spatial cutoff frequencies of the filter are discussed in Sec. III B 3.

The range is then estimated based on the slope of the striations in the window. This process is repeated for several windows located on a grid in the (r, f) plane. Each window on the grid will produce one range estimate, all of which can then be averaged obtain a single, robust estimate. Note that the vertical axis of the window is frequency, so it requires that the source be broadband. The horizontal axis of the window is range, and so it requires that the acoustic field is measured along a line emanating radially from the acoustic source.

B. Determining local striation angle

Denote a rectangular window of $I(r, f)$ bounded by $(r_{\min} < r < r_{\max})$ and $(f_{\min} < f < f_{\max})$ as $I_{\text{win}}(r, f)$. The striations inside of $I_{\text{win}}(r, f)$ will all have approximately the same slope if the window size is sufficiently small.

Several articles have pointed out the relationship between the 2D-DFT of $I_{\text{win}}(r, f)$ and the slope of the striations in $I_{\text{win}}(r, f)$.^{4-6,10} That relationship forms the basis for the approach used in the present work to determine the local striation angle. The process of determining the local striation angle involves five main steps:

- (1) Take a 2D-DFT of $I_{\text{win}}(r, f)$.
- (2) Eliminate regions of the 2D-DFT of $I_{\text{win}}(r, f)$ associated exclusively with noise content.
- (3) Convert the 2D-DFT of $I_{\text{win}}(r, f)$ to polar coordinates.
- (4) For several hypothesized striation angles, add up (integrate) all of the components of the 2D-DFT of $I_{\text{win}}(r, f)$ corresponding to that striation angle.
- (5) The striation angle that has the most “energy” is then the estimate.

These steps are illustrated in Fig. 2 and are described in detail in Secs. III B 1–III B 4. The steps are related to the Radon transform and the Fourier-slice theorem.¹¹ If one were to skip the second step, then the steps could be performed with a Radon transform using the Fourier-slice theorem.¹² But because step 2 eliminates components of $I_{\text{win}}(r, f)$ above particular spatial frequencies, this analysis works directly with the 2D-DFT of $I_{\text{win}}(r, f)$.

1. Interpretation of the two-dimensional discrete Fourier transform

$I_{\text{win}}(r, f)$ has striations whose slope needs to be determined in order to estimate the source’s range. Figure 2(a) shows an example $I_{\text{win}}(r, f)$. Denote the magnitude of the 2D-DFT of $I_{\text{win}}(r, f)$ as $I_{2\text{DF}}(k_r, k_f)$,

$$I_{2\text{DF}}(k_r, k_f) = \left| \iint \int I_{\text{win}}(r, f) e^{-j2\pi(k_r r + k_f f)} dr df \right|.$$

Note that in this paper k_r and k_f refer *not* to the wavenumbers of the acoustic wave, but to the wavenumbers of the “image”

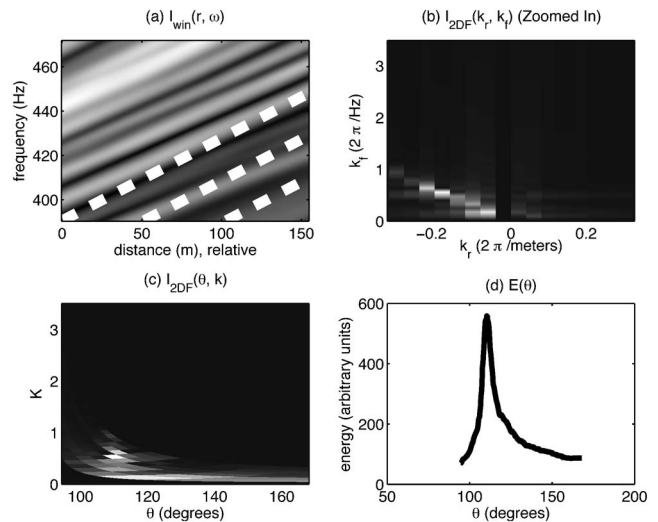


FIG. 2. The steps used to determine the angle of the striations in $I_{\text{win}}(r, f)$. (a) shows $I_{\text{win}}(r, f)$, a window of $I(r, f)$. The two-dimensional Fourier transform of $I_{\text{win}}(r, f)$ is then taken resulting in $I_{2\text{DF}}(k_r, k_f)$, shown in (b) (using the bounds described in Sec. III B 3). $I_{2\text{DF}}(k_r, k_f)$ is then converted into polar coordinates, $I_{2\text{DF}}(\theta, K)$, shown in (c). $I_{2\text{DF}}(\theta, K)$ is then integrated along K to produce $E(\theta)$, shown in (d). The angle corresponding to the peak of $E(\theta)$ is then the estimated angle of the striation. White dotted lines corresponding to the estimated striation angle are plotted in (a) for visual comparison.

$I_{\text{win}}(r, f)$. Hence, k_r and k_f will be referred to as the image wavenumbers. They are the horizontal and vertical axes, respectively, of Fig. 2(b). In Sec. III B 3, the relationship between k_r and k_f and the acoustic horizontal wavenumbers of the modes propagating in the waveguide will be derived.

In practice one has a discrete (sampled) version of $I(r, f)$, so the two-dimensional Fourier transform is implemented as a two-dimensional discrete Fourier transform. The direction of the mainlobe originating from the origin of $I_{2\text{DF}}(k_r, k_f)$ is perpendicular to the slope of the striations in the window of $I(r, f)$. An example is shown in Figs. 2(a) and 2(b). (They do not appear exactly perpendicular because of the different aspect ratios of the figures.)

If one thinks of $I_{\text{win}}(r, f)$ as an image, ignorant of the fact that it represents power spectrum of an acoustic field, then its 2D-DFT, $I_{2\text{DF}}(k_r, k_f)$, can be interpreted as a decomposition of $I_{\text{win}}(r, f)$ into “cosine” image basis functions, each with a unique image wavenumber.^{13,14}

The acoustician may gain insight by noting that the basis functions of a 2D-DFT of an image look like two-dimensional plane waves with the time dependence removed: $\exp(j(k_x x + k_y y))$.

Each pixel of $I_{2\text{DF}}(k_r, k_f)$ represents a single basis function with image wavenumbers of k_r and k_f [horizontal and vertical image wavenumbers, respectively, in Fig. 2(a)]. One may find this easier to understand if she or he ignores that r and f represent range and frequency, and instead thinks of them simply as labels for the x and y axes of Fig. 2(a).

To relate k_r and k_f to striation angles, one can interpret each combination of k_r and k_f [or each pixel of Fig. 2(b)] as representing a cosine basis function at a particular angle with a particular period (striation width).

2. Application of the 2D-DFT to determine striation angle

The waveguide invariant, as shown in Eq. (2), makes a statement only about the slopes of the striations; it says nothing about the distance between the striations. From an image processing perspective, the waveguide invariant makes a statement about the angle of the basis functions comprising $I_{\text{win}}(r, f)$; it says nothing about the period (striation width) of those image basis functions. But as Chuprov pointed out in his original derivation of the waveguide invariant, one can calculate the minimum striation width using only modest information about the waveguide. This allows one to filter out noise by only including components of $I(r, f)$ with image wavenumbers less than the maximum expected due to the acoustic source of interest, as will be discussed in Sec. III B 3.

To determine the angle of the striations in $I_{\text{win}}(r, f)$, we first remove the mean of $I_{\text{win}}(r, f)$ and then take its 2D-DFT to obtain $I_{2\text{DF}}(k_r, k_f)$. Then we transform $I_{2\text{DF}}(k_r, k_f)$ from Cartesian coordinates to polar coordinates:

$$I_{2\text{DF}}(k_r, k_f) \Rightarrow I_{2\text{DF}}(\theta, K), \quad (4)$$

where

$$\theta = \arctan(k_f/k_r), \quad K = \sqrt{k_r^2 + k_f^2}.$$

Note that it is legitimate to add k_r and k_f together because they are dimensionless, as they are the result of the 2D-DFT. However, throughout most of the present work k_r and k_f are “redimensionalized” based on the sampling used in the 2D-DFT, just as is typically done with power spectra based on discretely sampled temporal waveforms.

Nearest-neighbor interpolation is used to do the coordinate transform. An example $I_{2\text{DF}}(\theta, K)$, is shown in Fig. 2(c).

If one places bounds on the possible ranges to the acoustic source, one can use Eq. (2) to put bounds on the angles that could have striations due to the waveguide invariant. The present analysis assumes the source was between 100 and 5000 m. Typically this only eliminates a few degrees (e.g., angles of 3°–87°, instead of 0°–90°), but the striation angle finding algorithm benefits from this because it occasionally incorrectly chooses very steep or very shallow angles as the dominant striation angle.

$$\theta_{\min} = \arctan\left(\frac{\text{maximum frequency in window}}{\text{minimum range to search}}\right),$$

$$\theta_{\max} = \arctan\left(\frac{\text{minimum frequency in window}}{\text{maximum range to search}}\right)$$

Interpolation is not strictly necessary to obtain the value of $I_{2\text{DF}}(\theta, K)$ at an arbitrary (θ, K) . One can evaluate the 2D-DFT of a sampled version of $I(r, f)$ at arbitrary k_r and k_f values, analogous to a discrete time Fourier transform for a discrete time series. However, doing this is computationally intensive because one cannot utilize the fast Fourier transform algorithm, and the present analysis did not suggest a noticeable increase in striation-angle finding performance when doing this to avoid interpolation.

$I_{2\text{DF}}(\theta, K)$ is then integrated along the K direction [the y -axis in Fig. 2(c)] to add up all the components of the image with a particular striation angle [remembering that $I_{2\text{DF}}(\theta, K)$ will already have been spatially filtered to eliminate high frequency noise].

$$E(\theta) = \int I_{2\text{DF}}(\theta, K) dK. \quad (5)$$

$E(\theta)$ approximately represents the amount of energy (in an image processing sense, not in an acoustic sense) in $I_{2\text{DF}}(k_r, k_f)$ of striations at a particular angle in $I(r, f)$. A plot of an $E(\theta)$ is shown in Fig. 2(d). Note that a proper change of variables would give an extra factor of K on the right hand side of Eq. (5), as noted in Ref. 4. Because the present analysis does not have that extra factor of K , lower values of K are weighted more heavily. The precise meaning of this can be seen by looking at the mapping between pixels in Figs. 2(b) and 2(c). This was done because it led to better estimates of the striation angle.

Finally, the angle corresponding to the maximum value of $E(\theta)$ is the most dominant angle in the basis functions comprising $I_{\text{win}}(r, f)$. The angle of the striations is perpendicular to the angle of the basis function:

$$\theta_{\text{striation}} = \arg \max_{\theta} E(\theta) + \pi/2. \quad (6)$$

An $I_{2\text{DF}}(k_r, k_f)$ obtained from experimental data will have noise at all values of k_r and k_f . However, the region of $I_{2\text{DF}}(k_r, k_f)$ that is important for the slope estimation (the signal of interest) lies mostly at lower values of k_r and k_f . It was found that even at very high signal-to-noise ratios, the noise can significantly deteriorate the slope estimate because the maximum value of k_r and k_f represented $I_{2\text{DF}}(k_r, k_f)$ can be arbitrarily large depending on how finely $I(r, f)$ was sampled in range and frequency. The effect of the noise can be reduced significantly by limiting the region of integration of Eq. (5) to $(-k_{r,\max} < k_r < k_{r,\max})$ and $(0 < k_f < k_{f,\max})$. Section III B 3 will demonstrate how to choose $k_{r,\max}$ and $k_{f,\max}$.

3. Upper bounds on k_r and k_f

Chuprov⁶ showed that one can relate the environmental parameters of the waveguide to the maximum rate at which $I(r, f)$ can oscillate in r and in f . In this subsection, we reproduce the results from Ref. 6 in the context of the problem at hand—source range estimation in a shallow-water waveguide. Determining an upper bound on the rate at which $I(r, f)$ oscillates in r and in f is equivalent to determining an upper bound on the k_r and k_f due to the acoustic source of interest. Any components of $I_{2\text{DF}}(k_r, k_f)$ above some $k_{r,\max}$ and $k_{f,\max}$ can be regarded as noise because they cannot be due to the source of interest.

In order to exclude as much noise as is possible, the integration in Eq. (5) of $I_{2\text{DF}}(k_r, k_f)$ will be bounded by $k_{r,\max}$ and $k_{f,\max}$. An example of this region is shown in Fig. 3. Note that this is equivalent to low-pass filtering the image.

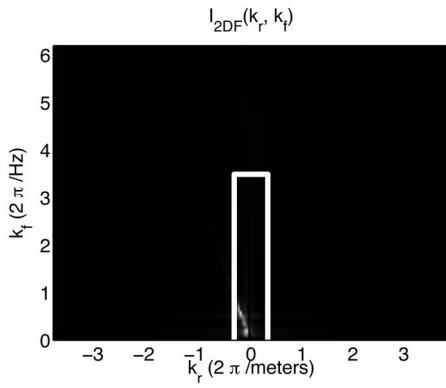


FIG. 3. $I_{2DF}(k_r, k_f)$ showing the full range of k_r and k_f , with white lines illustrating the bounds described in Sec. III B 3. This figure illustrates why it is essential to limit the region of integration in Eq. (5). Even if the noise outside the white lines is at a low level, it can dominate the integral in Eq. (5) because of the large ratio of outer to inner areas separated by the white lines. The inner area is what is shown in Fig. 2(b).

According to Eq. (1), the acoustic intensity is a sum of cosines. Each cosine term has an image wavenumber in the r direction of

$$k_{r(mn)} = \frac{\partial(\Delta\xi_{mn}(f)r)}{\partial r} = \Delta\xi_{mn}(f) \quad (7)$$

and an image wavenumber in the f direction of

$$k_{f(mn)} = \frac{\partial(\Delta\xi_{mn}(f)r)}{\partial f} = \frac{r \partial(\Delta\xi_{mn}(f))}{\partial f}. \quad (8)$$

An upper bound on $k_{r(mn)}$ in $I(r, f)$ can be determined (to within the approximations used when deriving the waveguide invariant) by calculating the largest possible value of $\xi_{mn}(f)$. All nonzero values in $I_{2DF}(k_r, k_f)$ with k_r image wavenumbers above the maximum value of $\xi_{mn}(f)$ are likely due to noise, and can be excluded from the integration in Eq. (5). For all ocean acoustic waveguides, the horizontal wavenumbers are bounded by

$$\left[\frac{2\pi f}{c_{\max}}, \frac{2\pi f}{c_{\min}} \right], \quad (9)$$

where c_{\max} and c_{\min} are the respective maximum and minimum sound speeds that occur in the environment. Thus

$$k_{r, \max} = 2\pi f \left(\frac{1}{c_{\min}} - \frac{1}{c_{\max}} \right). \quad (10)$$

To determine an upper bound on $k_{f(mn)}$, we use Eq. (8) and replace f with $\omega/(2\pi)$, and note that $\partial\xi_{mn}/\partial\omega$ is the reciprocal of the group speed of mode m . The maximum and minimum group speeds are bounded by fastest and slowest media in the waveguide, so

$$k_{f, \max} = 2\pi r \left(\frac{1}{c_{\min}} - \frac{1}{c_{\max}} \right). \quad (11)$$

These upper bounds are used to limit the region of integration in Eq. (5). Using Eqs. (11) and (10), one can set the

bounds loose enough to include virtually all realistic ocean waveguides on Earth but still reject much of the noise in $I_{2DF}(k_r, k_f)$. The r in Eq. (11) should be set to the maximum range that one expects to see the source. All results presented in this paper used Eqs. (10) and (11) with $r=5000$ m, $c_1=1500$ m/s, and $c_2=1800$ m/s.

4. Choosing the window size

$I_{\text{win}}(r, f)$ is a rectangular window of $I(r, f)$, bounded by ($r_{\min} < r < r_{\max}$) and ($f_{\min} < f < f_{\max}$), inside of which the striation slope will be estimated using a 2D-DFT. The purpose of this section is to determine how one goes about choosing the window size. Denote the window size by

$$\Delta f = f_{\max} - f_{\min}, \quad (12)$$

$$\Delta r = r_{\max} - r_{\min}. \quad (13)$$

To accurately determine the striation angle, the observation window of $I(r, f)$ must be large enough in r and f such that at least one full striation (from peak to trough to peak) is contained within the window, in each direction (r and f). The statement in the previous sentence can be quantified by noting that the frequency resolution of the DFT for some variable x is $\Delta k_x = 2\pi/\Delta x$, so if the DFT of a signal is to distinguish the frequency of k_x from the zero frequency, then one needs to observe at least $\Delta x = 2\pi/k_x$.

In theory one could use the $k_{r, \max}$ derived Sec. III (originally derived in Ref. 6) to determine the minimum Δr . However, only one term in the sum in Eq. (1) will lead to such a high value of k_r . So using $k_{r, \max}$ would underestimate the minimum Δr that is required to estimate the striation slope in practical situations. A better way to determine the minimum value of Δr is to use the value of $k_{r(mn)}$ averaged over m and n .

To do this, first the approximate values of $\Delta\xi_{mn}(f)$ for an ideal waveguide will be calculated. Then the additional approximations required for nonideal waveguides will be discussed. For an ideal waveguide, the difference in horizontal wavenumbers of modes not near cutoff can be written as (Sec. 6.7.2 of Ref. 7)

$$\Delta\xi_{mn}(f) = \xi_m(f) - \xi_n(f) \approx \frac{1}{2} \left(\frac{c}{2\pi f} \right) \left(\frac{\pi}{d} \right)^2 (m^2 - n^2). \quad (14)$$

Note that because the intensity is a sum of cosines and $\cos(\Delta\xi_{mn}r) = \cos(-\Delta\xi_{mn}r)$, only the absolute value of $\Delta\xi_{mn}$ is of interest. The average absolute value of the wavenumber differences can be determined by calculating the average value of $|m^2 - n^2|$:

$$\overline{|n^2 - m^2|} = \frac{1}{M^2} \sum_{n=1}^{n=M} \sum_{m=1}^{m=M} |n^2 - m^2| = \frac{M^4 + M^3 - M^2 - M}{3M^2}, \quad (15)$$

where M is the number of propagating modes. The computer algebra system MATHEMATICA was used to determine the formula for the sum. For $M \gg 1$,

$$\overline{(n^2 - m^2)} \approx \frac{1}{3}M^2. \quad (16)$$

For an ideal waveguide, Eq. (16) can be inserted into Eq. (14) to determine the approximate average horizontal wavenumber difference and thus the average value of the image wavenumber k_r .

For nonideal waveguides, this analysis assumes that the horizontal wavenumber differences are distributed similarly to that of an ideal waveguide, but are bounded by the maximum and minimum k in the media:

$$\Delta\xi_{mn}(f) = 2\pi f \left(\frac{1}{c_{\min}} - \frac{1}{c_{\max}} \right) \frac{n^2 - m^2}{M^2}. \quad (17)$$

The mean horizontal wavenumber difference is then

$$\overline{k_{r(mn)}(f)} = \overline{\Delta\xi_{mn}(f)} = 2\pi f \left(\frac{1}{c_{\min}} - \frac{1}{c_{\max}} \right) \frac{1}{3}. \quad (18)$$

Conveniently, this does not depend on M .

For the average value of k_f , we use a similar argument. Beginning with Eqs. (8) and (14),

$$\overline{k_{f(mn)}} = r \frac{\partial(\overline{\Delta\xi_{mn}(f)})}{\partial f} = \left(\frac{rc\pi}{4d^2f^2} \right) \overline{(m^2 - n^2)} = \left(\frac{rc\pi}{4d^2f^2} \right) \frac{M^2}{3}, \quad (19)$$

one can then insert M for an ideal waveguide.

For nonideal waveguides, this analysis assumes that the derivative of the horizontal wavenumbers with respect to f are distributed similarly to that of an ideal waveguide (or equivalently, the group slownesses are distributed similarly to that of an ideal waveguide), bounded by the minimum and maximum group slownesses. In that case, the mean $k_{f(mn)}$ is

$$\overline{k_{f(mn)}} = 2\pi r \left(\frac{1}{c_{\min}} - \frac{1}{c_{\max}} \right) \frac{1}{3}. \quad (20)$$

Equations (18) and (20) can be used to ensure that the window will contain one full striation of the *average* striation width. A larger window size could be used and could potentially lead to a more accurate striation slope estimate because the resolution of the 2D-DFT is inversely proportional to the window size. But because the slopes of the striations contained in $I(r, f)$ change with r and f according to Eq. (2), the window size should not be too large or it will contain striations with a wide range of slopes.

We now discuss how to choose the window size, given the trade-offs mentioned in the previous paragraph.

$I_{\text{win}}(r, f)$ will contain striation slopes ranging from f_{\min}/r_{\max} to f_{\max}/r_{\min} . One way to choose the window size would be to make the range of striation slopes in the window equal the range of striation slopes represented by the 2D-DFT bin. According to Eq. (2), a window of size Δr by Δf centered at r and f will have slopes ranging from

$$\frac{f + \Delta f/2}{r - \Delta r/2} \quad \text{to} \quad \frac{f - \Delta f/2}{r + \Delta r/2}. \quad (21)$$

A striation's slope is perpendicular to the angle (in r, f space) of its cosine basis function, so an image wavenumber

of k_r and k_f represents a striation with a slope of $-k_r/k_f$. Thus, an image wavenumber frequency bin of size Δk_r by Δk_f located at k_r and k_f represents striations ranging from

$$-\frac{k_r + \Delta k_r/2}{k_f - \Delta k_f/2} \quad \text{to} \quad -\frac{k_r - \Delta k_r/2}{k_f + \Delta k_f/2}. \quad (22)$$

To make the range of striation slopes in the window equal the range of striation slopes represented by the 2D-DFT bin, one could in principle substitute $k_r = 2\pi/\Delta r$ and $k_f = 2\pi/\Delta k_f$ into Eqs. (21) and (22), and then set the ranges of slopes equal to each other. The solution would depend on k_r and k_f , for which one could use the average values derived in this section. The solution would also depend on r , for which one could choose some value in the middle of the search range. An exact analytic solution can be obtained and would ensure that the range of slopes represented by the 2D-DFT bin would equal the range of slopes in the window. However, doing so will only provide a relationship between Δr and Δf , not values for both quantities because there are an infinite number of combinations of Δr and Δf that could satisfy the equality.

A less quantitatively rigorous but more pragmatic approach is used in the present work to determine the value of Δr and Δf . We start with the heuristic that the window should be roughly three times the average striation width that we expect to see in each direction. This heuristic is motivated by a desire for the 2D-DFT bin representing the average image wavenumber expected to be a few 2D-DFT bin widths away from both axes in Fig. 2(b). Thus we desire

$$\Delta r = \frac{3 \cdot 2\pi}{k_{f(mn)}}, \quad \Delta f = \frac{3 \cdot 2\pi}{k_{r(mn)}(f)}. \quad (23)$$

The r in Eq. (20) should be set toward the lower end of the ranges over which one is searching for the source.

In the present work, Δf was determined by using Eqs. (23) and (20) with $c_1 = 1500$ m/s, $c_2 = 1800$ m/s, and $r = 1000$ m, resulting in $\Delta f \approx 81$ Hz. Δr was determined by using Eqs. (23) and (18) with $c_1 = 1500$ m/s, $c_2 = 1800$ m/s, and $f = 525$ Hz (the middle of the frequency range of the data presented in the next section), resulting in $\Delta r \approx 154$ m.

The parameter values determined in this section— $k_{r, \max}$, $k_{f, \max}$, Δf , and Δr —are used to process the simulated and both experimental data sets. The parameter values were not “fine tuned” for each data set, illustrating the robustness of the method to the choice of the parameters. In fact, it was observed that all of the parameters can be adjusted by roughly a factor of 2 (increase or decrease) without drastically affecting the results for the data sets analyzed in the present paper.

Equations (18), (20), and (23) provide practical estimates of the minimum source bandwidth and minimum horizontal aperture required for range estimation. These estimates are shown to be accurate with experimental data in Sec. IV B. However, it is important to keep in mind that Eqs. (18), (20), and (23) were derived for range independent waveguides. Under some circumstances (e.g., a rough sea

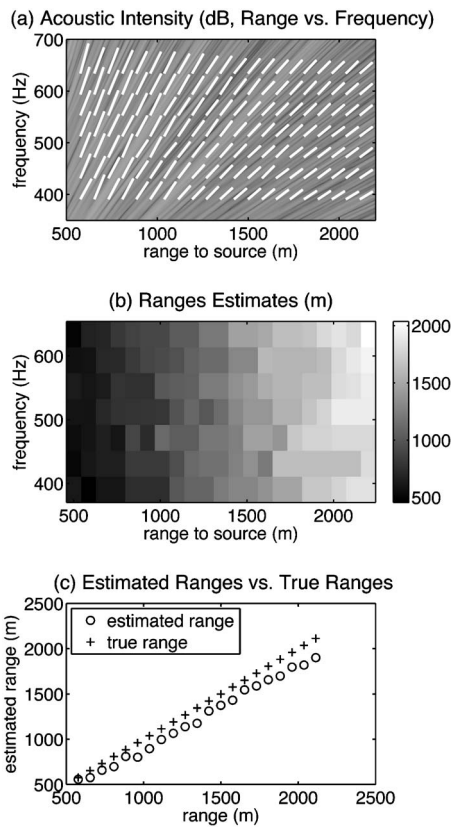


FIG. 4. Range estimates for a simulated Pekeris waveguide. (a) Same as Fig. 1, but with the estimated slopes superimposed as white solid lines. (b) Range estimates based on each slope in (a) plotted versus the true range. (c) Range estimates versus true range, obtained by averaging each column of (b). The bias is discussed Sec. IV A.

surface, or a source with a high temporal frequency f), effects such as incoherent scattering will smear out the high image-wavenumber striations, and a window larger than that predicted by Eq. (23) will be necessary to estimate a striation's slope.

IV. RESULTS

A. 2D-DFT technique applied to simulated data

In this subsection, the striation angle finding technique based on the 2D-DFT is tested on the simulated acoustic intensity plot shown in Fig. 1. Equation (3) is then used to estimate the range to the acoustic source, assuming $\beta=1$.

First, $I(r, f)$ is divided into several windowed segments, $I_{\text{win}}(r, f)$, spread on a grid throughout the (r, f) plane. The striation angle is then estimated in each $I_{\text{win}}(r, f)$ using the technique described in Sec. III.

The resulting slope estimates are shown in Fig. 4(a). Each slope estimate is associated with a range estimate, which are shown in Fig. 4(b).

In order to use all of the data, one needs to ensure that every pixel in Fig. 1 is contained inside at least one window. In fact, one can let the windows overlap. In this paper, the windows overlapped by about 50% in both the r and the f directions.

One can average each column of Fig. 4(b) to obtain

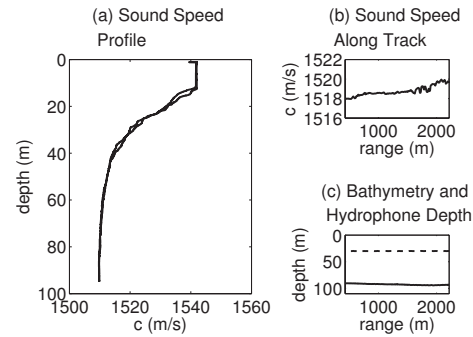


FIG. 5. (a) Sound speed profiles taken before and after the acoustic data collection. (b) Sound speed at the hydrophone's depth plotted versus range along the track. (c) Water column depth (solid line) and hydrophone depth (dashed line) plotted versus range from the source along the hydrophone's path.

more accurate range estimates. The result of such averaging, plotted versus the true range to the source, is shown in Fig. 4(c).

The estimates are biased by about 10%. This is most likely due to the fact that the derivation of the waveguide invariant does not take into account the $1/r$ cylindrical spreading, which will cause the actual slopes to be steeper than that predicted by the waveguide invariant. However, it could also be due to the other approximations made when the waveguide invariant, such as the dependence of the mode shapes on frequency. Because this error is less than the expected range estimate accuracy for experimental data, it will not be addressed further in the present analysis.

B. 2D-DFT technique applied to experimental data

The experimental data presented in this paper was collected during GLINT08, an experiment performed during the summer of 2008 near Pianosa Island, Italy. Two sound speed profiles measured about 1 h before and 1 h after the acoustic data were collected are shown in Fig. 5(a), but note that this information was not used by the range estimation algorithm.

An acoustic source was lowered 40 m below the ocean surface from a research vessel that was using dynamic positioning to keep its position as fixed as possible. Due to a malfunctioning GPS unit, the acoustic source's position had an uncertainty of 100 m. The signal projected from the source was pseudorandom white noise with an approximately flat spectrum from 300 to 750 Hz and a frequency-integrated source level of 150 dB re 1 μPa at 1 m. Due to equipment limitations, the signal was a single 65 000 point realization of white noise that was repeated back-to-back every 5.33 s.

An acoustic receiver was towed directly toward the acoustic source from a range of 2200 m to about 500 m at a speed of 1.5 m/s and at a depth of 30 m. This segment of the experiment is referred to as the incoming segment. The acoustic receiver was then lowered to 50 m, and towed away from the source at 1.5 m/s back out to a range of 2200 m. This segment is referred to as the outgoing segment. The acoustic receiver was moving continuously, so all of the presented data were collected in less than 1 h. There was a small Doppler shift of about 1% due to receiver motion. Such a

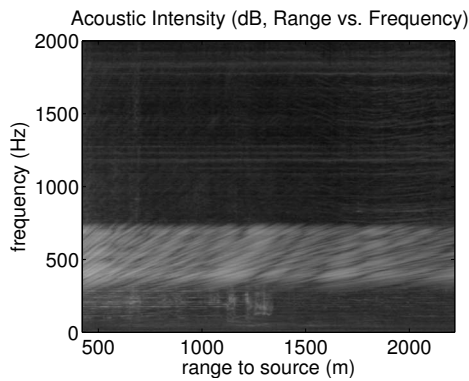


FIG. 6. The acoustic intensity (dB, arbitrary reference) as measured by the acoustic receiver for the incoming segment of the experiment. The striations are clearly visible in the frequency range of the source, from 350 to 700 Hz.

shift may cause range estimate errors of about 1%, which is negligible compared to the overall expected accuracy and thus will be ignored. The acoustic receiver location had an uncertainty of 50 m.

The acoustic data were sampled at a frequency of 4 kHz. The window length used to estimate the spectrum of the received signal had to be 21 334 points long so that it corresponded to the 5.33 s repetition rate of the signal. Under other circumstances, one would be free to choose other window lengths that do not strongly depend on the signal characteristics. Because the acoustic receiver was moving at an approximately 1.5 m/s, each spectrum (each column of Fig. 6) represents $\approx 5.33 \text{ s} \times 1.5 \text{ m/s} = 8 \text{ m}$ in distance that the acoustic receiver traveled. The Blackman–Tukey method of spectrum estimation was used to estimate each spectrum (each column of Fig. 6). Because the acoustic receiver was towed at an approximately constant rate, the spectrogram of the recorded time series is $I(r, f)$.

Once the spectrogram, $I(r, f)$, was calculated, the processing method was exactly the same as that used for the simulated data. The same parameter values were used.

1. Incoming segment

The water column depth, acoustic receiver's depth, and sound speed along the hydrophone's path are plotted in Figs. 5(b) and 5(c). The measured acoustic field from 0 Hz to 2 kHz is shown in Fig. 6. The results of the range estimation algorithm are shown in the same format as the simulated results, in Figs. 7(b) and 7(c).

There is extremely good qualitative agreement between the angle determined by the striation angle finding algorithm and the striation angle as it appears to a human observer, as can be seen in Fig. 7(a). At source ranges larger than 1000 m, the estimated range tends to be less than the true range. This could be the result of any number of effects, including three-dimensional propagation effects, range inhomogeneities, the temporal stationarity of the SSP while the field was being measured, and the approximations used when deriving the waveguide invariant. Section IV C shows a simulated spectrogram for comparison.

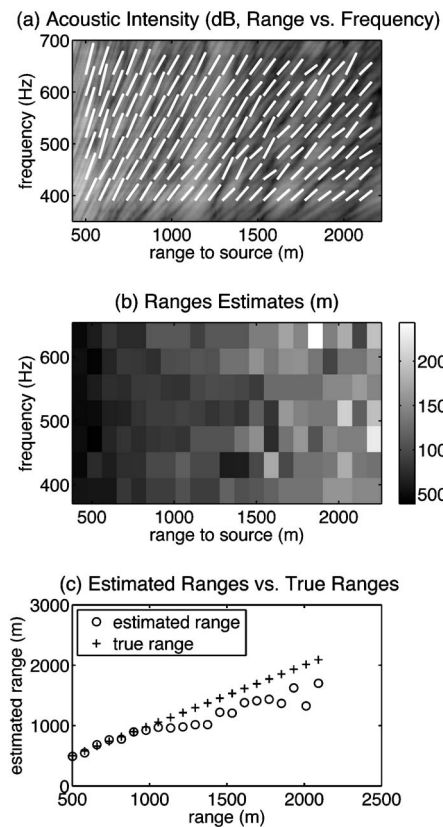


FIG. 7. Range estimates for the incoming segment of the experiment. (a) A zoom-in of Fig. 6 on the frequencies of interest, with the estimated slopes superimposed as solid white lines. (b) Range estimates based on each estimated slope in (a), plotted versus the true range. (c) Range estimates versus true ranges, obtained by averaging each column of (b).

2. Outgoing segment

The watercolumn depth and sound speed along the hydrophone's path were similar to the incoming segment (see Fig. 5). The measured acoustic field, from 0 to 2 kHz is shown in Fig. 8. There is a loud interfering broadband acoustic source during the portion of the spectrogram corresponding to a range of 1000–2000 m. As one can see in Fig. 9, this does affect the estimates, but not as much as one might expect. The estimates are only adversely affected at ranges of 1400–1800 m, when the striations in the spectrogram from

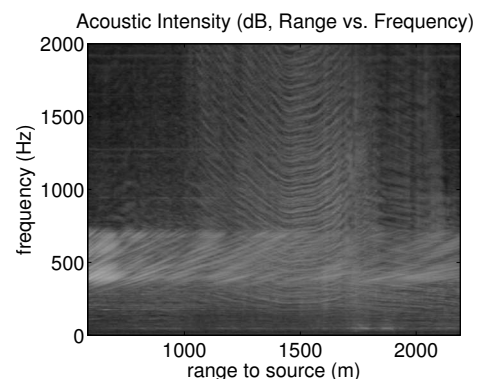


FIG. 8. The acoustic intensity (dB, arbitrary reference) as measured by the acoustic receiver along its track away from the source. Note the striations in the frequencies of the acoustic source (350–700 Hz) and the interfering source present during times corresponding to ranges from 1000 to 2000 m.

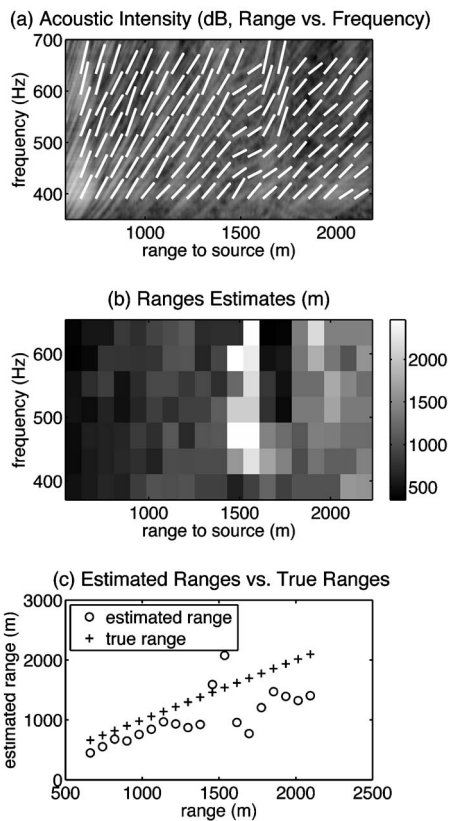


FIG. 9. Range estimates for the outgoing segment of the experiment. (a) A zoom-in of Fig. 8 on the frequencies of interest, with the estimated slopes superimposed as solid white lines. (b) Range estimates based on each estimated slope in (a), plotted versus the true range. (c) Range estimates versus true range, obtained by averaging each column of (b). Large errors occur when the interfering source was present.

the interferer are nearly parallel to the striations that are expected from the experimental acoustic source. If one did not know *a priori* that the acoustic receiver was moving away from the acoustic source of interest, then the estimates may have been affected more adversely because one would have had to search over the full 180° . The range estimates are accurate within a few hundred meters, excluding the estimates when the true range was 1400–1800 m.

C. Validity of $\beta=1$ assumption

In Sec. II, it was discussed that although usually $\beta \approx 1$ in shallow-water environments, that may not always be the case (see Ref. 4 for more details). All of the analysis in the present work assumed $\beta=1$, so it is worthwhile to simulate the acoustic field in an environment similar to the environment where the experimental data were collected, in order to determine if β differs significantly from the assumed value. (We expect it not to, otherwise we would not have been able to accurately estimate the range to the source in Sec. IV B.)

To do this, the normal mode program KRAKEN (Ref. 15) was used. The sound speed profile used was that collected during the experiment [shown in Fig. 5(a)]. The source and receiver geometry were the same as the incoming portion of the experiment. Because the bottom bathymetry and the sound speed profile changed very little with range, the environment was modeled as being range independent. The bot-

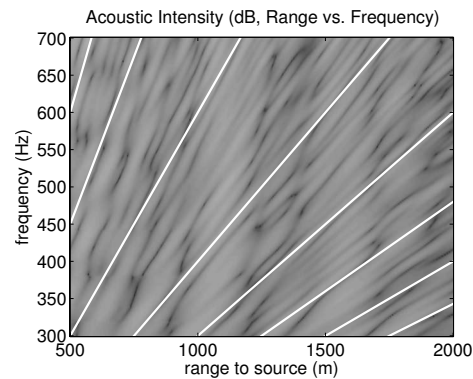


FIG. 10. A simulated spectrogram for the environment used to collect the experimental data. The white lines correspond to $\beta=1$. Most of the striations correspond to $\beta \approx 1$, with a few exceptions.

tom properties were unknown so typical values for a bottom half-space were used ($c_{\text{bottom}}=1650$ m/s, $\rho_{\text{bottom}}=1.5$ g/cm³, $\alpha=0.5$ dB/ λ).

Figure 10 shows the simulated spectrogram. The white lines have slopes corresponding to $\beta=1$. It can be seen that there are some striations with slopes that are slightly steeper than the $\beta=1$ lines, but almost no striations have slopes that are shallower than the $\beta=1$ lines. This could explain why the ranges tended to be underestimated in some parts of the incoming segment of the experiment [Fig. 7(c)], and suggests that β may have a value slightly larger than one for this particular environment and source-receiver geometry.

The fact that the range estimates from the experimental data in Fig. 7(c) were between about 75% and 100% of the true range implies that β had a value between about 1 and 4/3 for the environment where the experimental data were collected.

Determining when one can assume that $\beta \approx 1$ is still an active area of research, but some guidelines are given in Refs. 4 and 9, and other papers on the waveguide invariant.

V. SUMMARY AND CONCLUSION

A processing scheme based on the waveguide invariant and the 2D-DFT of $I(r, f)$ was used to estimate an acoustic source's range using simulated data and two sets of experimental data. The processing techniques used did not require human interpretation of any images in order to obtain the range estimate, making the techniques suitable for implementation on an autonomous platform.

A relationship between the average image wavenumbers in the 2D-DFT of $I(r, f)$ and the acoustic waveguide parameters was used to determine the minimum observation window size of $I(r, f)$ required for range estimation. A similar relationship was used to reject noise in $I(r, f)$.

The same set of signal processing parameter values (maximum image wavenumber, and window size in range and frequency) was used for both simulated and experimental data, showing that the signal processing parameters' values do not need to be fine tuned for each data set. The range estimates were based on the assumption that $\beta=1$ but were accurate to within about 25% despite using only a minimal amount of *a priori* knowledge about the environment. The

technique appeared to be robust, but more experimental data would be needed to determine the robustness of these algorithms in other environmental conditions.

ACKNOWLEDGMENTS

Thanks to Arjuna Balasuriya, Toby Schneider, and Kevin LePage. Thanks to the JASA reviewers for their many suggestions to strengthen this paper. Work sponsored by the Office of Naval Research under Grant No. N00014-08-1-0013.

- ¹A. B. Baggeroer, W. A. Kuperman, and H. Schmidt, "Matched field processing: Source localization in correlated noise as an optimum parameter estimation problem," *J. Acoust. Soc. Am.* **83**, 571–587 (1988).
- ²A. M. Thode, W. A. Kuperman, G. L. D'Spain, and W. S. Hodgkiss, "Localization using Bartlett matched-field processor sidelobes," *J. Acoust. Soc. Am.* **107**, 278–286 (2000).
- ³H. Tao, G. Hickman, J. Krolik, and M. Kemp, "Single hydrophone passive localization of transiting acoustic sources," in *IEEE OCEANS 2007—Europe* (2007).
- ⁴D. Rouseff and R. C. Spindel, "Modeling the waveguide invariant as a distribution," in *Ocean Acoustic Interference Phenomena and Signal Processing*, edited by W. A. Kuperman and G. L. D'Spain [AIP Conf. Proc. **621**, 137–150 (2002)].
- ⁵T. C. Yang, "Beam intensity striations and applications," *J. Acoust. Soc.*

Am. **113**, 1342–1352 (2003).

- ⁶S. D. Chuprov, "Interference structure of a sound field in a layered ocean," in *Ocean Acoustics: Current State*, edited by L. M. Brekhovskikh and I. B. Andreeva, (Nauka, Moscow, 1982).
- ⁷L. Brekhovskikh and Y. Lysanov, *Fundamentals of Ocean Acoustics*, 3rd ed. (AIP, New York/Springer, New York, 2003).
- ⁸G. L. D'Spain and W. A. Kuperman, "Application of waveguide invariants to analysis of spectrograms from shallow water environments that vary in range and azimuth," *J. Acoust. Soc. Am.* **106**, 2454–2468 (1999).
- ⁹J. E. Quijano, L. M. Zurk, and D. Rouseff, "Demonstration of the invariance principle for active sonar," *J. Acoust. Soc. Am.* **123**, 1329–1337 (2008).
- ¹⁰A. B. Baggeroer, "Modeling the waveguide invariant as a distribution," in *Ocean Acoustic Interference Phenomena and Signal Processing*, edited by W. A. Kuperman and G. L. D'Spain [AIP Conf. Proc. **621**, 151–170 (2002)].
- ¹¹A. C. Kak and M. Slaney, *Principles of Computerized Tomographic Imaging* (IEEE, New York, 1988).
- ¹²The authors thank an anonymous reviewer for pointing this out.
- ¹³J. M. Brayer, "Introduction to Fourier transforms for image processing," <http://www.cs.unm.edu/brayer/vision/fourier.html> (Last viewed 9/29/09).
- ¹⁴W. L. Briggs, *The DFT: An Owner's Manual for the Discrete Fourier Transform* (Society for Industrial and Applied Mathematics, Philadelphia, PA, 1995).
- ¹⁵M. B. Porter, "The kraken normal mode program," http://oalib.hlsresearch.com/Modes/AcousticsToolbox/manual_html/kraken.html (Last viewed 10/30/09).